

DOI: 10.1002/chem.201204064

Phenylethenyl-Substituted Triphenylamines: Efficient, Easily Obtainable, and Inexpensive Hole-Transporting Materials

Tadas Malinauskas,^[a] Maryte Daskeviciene,^[a] Giedre Bubniene,^[a] Ieva Petrikyte,^[a] Steponas Raisys,^[b] Karolis Kazlauskas,^{*[b]} Valentas Gaidelis,^[c] Vygintas Jankauskas,^[c] Robertas Maldzius,^[c] Saulius Jursenas,^[b] and Vytautas Getautis^{*[a]}

Abstract: Star-shaped charge-transporting materials with a triphenylamine (TPA) core and various phenylethenyl side arm(s) were obtained in a one-step synthetic procedure from commercially available and relatively inexpensive starting materials. Crystallinity, glass-transition temperature, size of the π -conjugated system, energy levels, and the way molecules pack in the solid state can be significantly influenced by variation of the structure of these side

arm(s). An increase in the number of phenylethenyl side arms was found to hinder intramolecular motions of the TPA core, and thereby provide significant enhancement of the fluorescence quantum yield of the TPA derivatives

in solution. On the other hand, a larger number of side arms facilitated exciton migration through the dense side-arm network formed in the solid state and, thus, considerably reduces fluorescence efficiency by migration-assisted nonradiative relaxation. This dense network enables charges to move more rapidly through the hole-transport material layer, which results in very good charge drift mobility (μ up to $0.017 \text{ cm}^2 \text{ V}^{-1} \text{ s}^{-1}$).

Keywords: amorphous materials • fluorescence spectroscopy • ionization potentials • luminescence • semiconductors

Introduction

Electronic and optoelectronic devices that use organic materials as active elements, for example, organic light-emitting diodes (OLED), organic photovoltaic devices (OPV), organic field-effect transistors (OFET), organic photoreceptors, and organic photorefractive devices, have received a great deal of attention from the standpoint of potential technological applications as well as fundamental science.^[1] Organic material devices are attractive because they can take advantage of low molecular weights, potentially low cost, and capability for thin-film, large-area, flexible device fabrication. All the devices described above involve charge transport as an essential operation process, and hence, require

proper charge-transporting materials. Therefore, the development of high-performance, charge-transporting materials is a key issue for the fabrication of high-performance devices.

Realization of the potential of organic electronics for simple processing requires the ability to form devices by solution deposition, preferably by using simple, inexpensive, easily purified materials. Among the low-molecular-weight organic compounds the highest charge-carrier mobilities in a single crystal were measured for rubrene ($\mu = 20 \text{ cm}^2 \text{ V}^{-1} \text{ s}^{-1}$).^[2] Pentacene showed the highest charge-carrier mobility in a polycrystalline film ($\mu \leq 5 \text{ cm}^2 \text{ V}^{-1} \text{ s}^{-1}$).^[3] However, pentacene is almost completely insoluble in common organic solvents, and therefore is processed solely by vacuum deposition. Thiophene derivatives have demonstrated very good charge mobilities ($\mu = 0.01\text{--}1 \text{ cm}^2 \text{ V}^{-1} \text{ s}^{-1}$),^[4] solubility, and processability. Their main drawback is relatively complicated and expensive multistep syntheses that involve organotin, organolithium, or organomagnesium reagents, expensive palladium or nickel catalysts, and rigorously anhydrous and oxygen-free conditions.^[2,5] Another large group of charge-transporting materials are nitrogen-containing triarylaminnes. These compounds have long been known as hole-transport materials (HTMs) for the active layer of organic photoreceptors, OLEDs, and organic solar cells. They show very good solubility in common organic solvents, stability towards air and humidity,^[2,5,6] and adequately high charge-carrier mobilities ($\mu = 0.01 \text{ cm}^2 \text{ V}^{-1} \text{ s}^{-1}$ in vapor-deposited,^[7] and spin-coated^[8] films). That said, however, it is important to emphasize that mobility results for the spin-coated films were obtained by

[a] Dr. T. Malinauskas, Dr. M. Daskeviciene, Dr. G. Bubniene, I. Petrikyte, Prof. V. Getautis
Department of Organic Chemistry
Kaunas University of Technology
Radvilenu pl. 19, Kaunas, 50254 (Lithuania)
Fax: (+370) 37-300152
E-mail: vytautas.getautis@ktu.lt

[b] S. Raisys, Dr. K. Kazlauskas, Prof. S. Jursenas
Institute of Applied Research
Vilnius University
Sauletekio 9-III, 10222, Vilnius (Lithuania)
E-mail: karolis.kazlauskas@ff.vu.lt

[c] Dr. V. Gaidelis, Dr. V. Jankauskas, Dr. R. Maldzius
Department of Solid State Electronics
Vilnius University
Sauletekio 9, Vilnius, 10222 (Lithuania)

Supporting information for this article is available on the WWW under <http://dx.doi.org/10.1002/chem.201204064>.

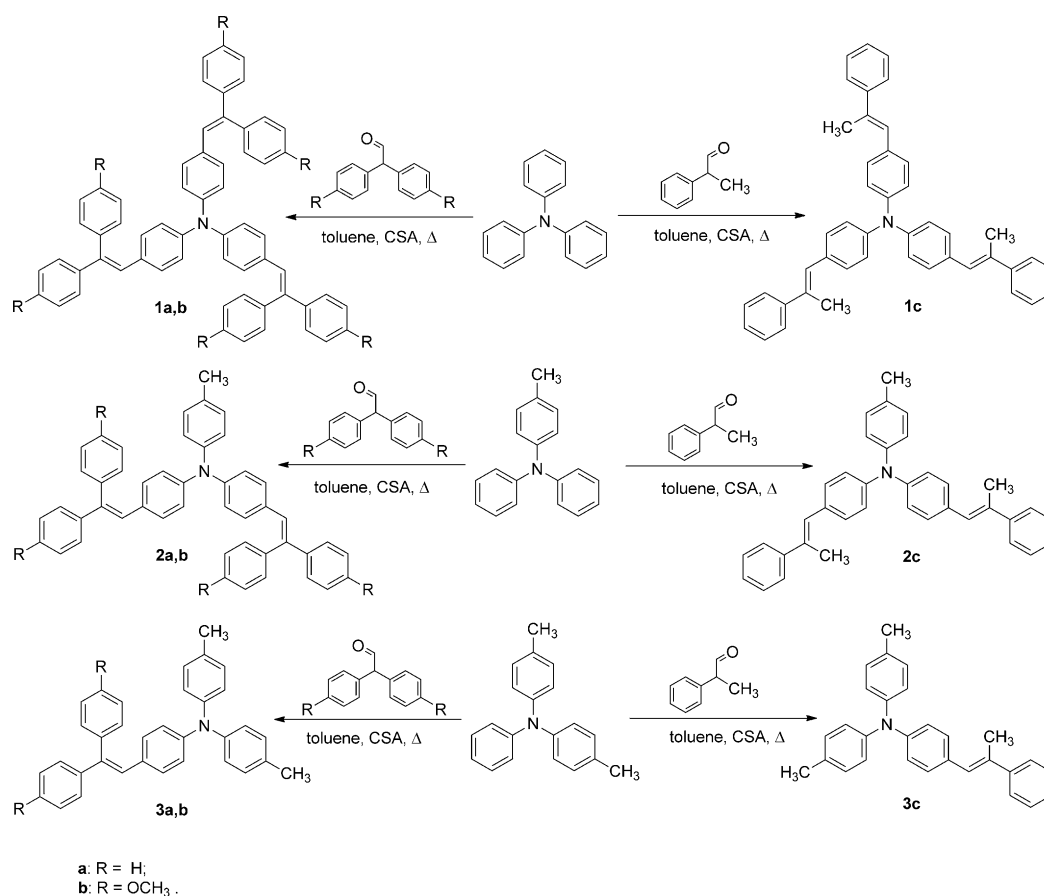
using conjugated polymers of triphenylamine (TPA). Polymeric materials have a number of important properties, such as ease of processing, normally very good film-forming properties, and high flexibility of the films. However, batch-to-batch variations in solubility, molecular weight, polydispersity, and purity can lead to different processing properties and performance. Small molecules contrast polymers in that they have well-defined molecular structures and definite molecular weights without any distribution. They can be purified by column chromatography, crystallization from solution, or by vacuum sublimation. All these factors allow for more reproducible fabrication protocols and a better understanding of molecular structure–property relationships. Currently, solution-processed, low-molecular-weight triarylamine derivatives demonstrate significantly lower results ($\mu \sim 10^{-4} \text{ cm}^2 \text{ V}^{-1} \text{ s}^{-1}$).^[9] Therefore, development of simple, inexpensive, easily purified, highly soluble triarylamine-based, low-molecular-weight compounds with optimal electronic properties remains an attractive and important goal.

Earlier, we have briefly reported the synthesis of star-shaped charge-transporting materials with a triphenylamine core and a variable number of diphenylethenyl side arms. These materials were obtained by simple synthetic procedures from inexpensive, commercially available starting materials, and demonstrated very good hole-transporting mobi-

lity.^[10] In this paper, we explore this concept in more depth. A number of new star-shaped charge-transporting materials with a triphenylamine core and a varied number of different phenylethenyl side arms have been synthesized. These hole-transporting organic semiconductors were obtained by the same one-step procedure reported earlier, from relatively inexpensive, commercially available or easily synthesized starting materials. The semiconductors can be solution processed and possess comparatively high charge drift mobility ($\mu = 0.017 \text{ cm}^2 \text{ V}^{-1} \text{ s}^{-1}$). Thermal, optical, and electronic properties of the TPA compounds were thoroughly evaluated and compared as a function of the number and type of phenylethenyl side arms.

Results and Discussion

Synthesis: The reported compounds were synthesized by condensation of the appropriate TPA derivative and relevant acetaldehyde in toluene (water generated in the course of the reaction was removed with a Dean–Stark trap). The mixture was heated at reflux in the presence of (\pm)-camphor-10-sulfonic acid (CSA) [Scheme 1]. Although compounds **3a–c** have already been reported in the literature^[11] they are included in this paper as reference materials and to



Scheme 1. Synthesis of phenylethenyl-substituted triphenylamines **1–3**.

demonstrate the scope and potential of the method. Similar compounds that contain phenylethenyl or diphenylethenyl fragments have been reported in the literature. However, they are obtained either by a multistep synthetic procedure that involves a McMurry cross-coupling reaction^[12a] or by palladium-catalyzed cross-coupling facilitated by a tailor-made ligand.^[12b]

Thermal properties: Isolated derivatives **1–3** are soluble in common organic solvents, such as THF, toluene, and chloroform. The thermal properties of **1–3** were determined by differential scanning calorimetry (DSC) (Figure 1, Table 1). The DSC measurements indicate that additional bulky phe-

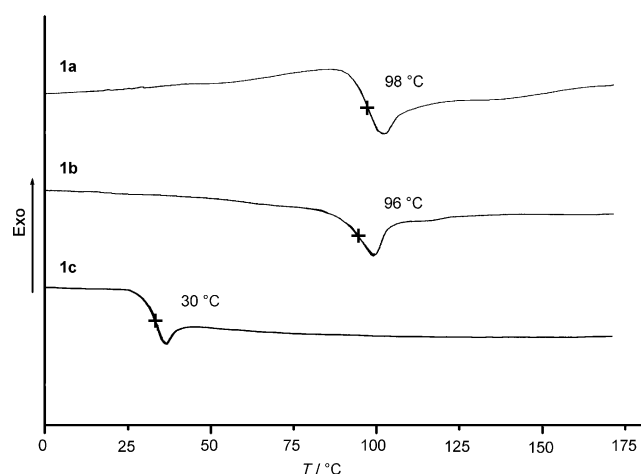


Figure 1. DSC second-heating curves for the TPA derivatives **1a–c**.

Table 1. Thermal characteristics of the synthesized derivatives.

| Compound | $T_g^{[a]}$ [°C] | M.p. ^[b] [°C] |
|-----------|------------------|--------------------------|
| 1a | 98 | 201 |
| 2a | 73 | – |
| 3a | – | 136 |
| 1b | 96 | – |
| 2b | 77 | – |
| 3b | 48 | 172 |
| 1c | 30 | – |
| 2c | 1 | – |
| 3c | 1 | – |

[a] Determined by DSC: scan rate = 10 K min⁻¹; N₂ atmosphere; second run. [b] M.p. was only detected during the first heating; the compound vitrified on cooling to rt with scan rate = 10 K min⁻¹.

nylethenyl fragments increase the glass-transition temperature (T_g) in all of the compounds investigated. Addition of methoxy groups has a very noticeable effect on the thermal characteristics of **3b**; its melting point is increased by 36 °C relative to **3a**, which allows it to form stable molecular glass.

Methoxy groups also introduce more structural disorder into **1b** relative to **1a**; **1b** is fully amorphous. Interestingly, however, the T_g values of **1b** and **2b** remain almost unchanged. Substitution of one phenyl ring with a methyl group lowers T_g close to (**1c**) or even below (**2c**) room tem-

perature. Due to their very low T_g values, **1c** and **2c** could be applied as plasticizers or as HTMs in applications in which good pore filling is needed, for example, solid-state dye-sensitized solar cells.^[13]

Monosubstituted TPA derivatives **3a–c** behave similarly to HTMs with two or three side arms. Diphenylethenyl-substituted compound **3a** is fully crystalline and does not form a stable amorphous state. Introduction of the methoxy groups in **3b** allows existence in both crystalline and amorphous states, whereas exchange of one phenyl ring for a methyl group in **3c** yields a fully amorphous material.

Optical properties: The absorption bands of compounds **1–3**, measured in THF, are shown in Figure 2 and summarized in Table 2.

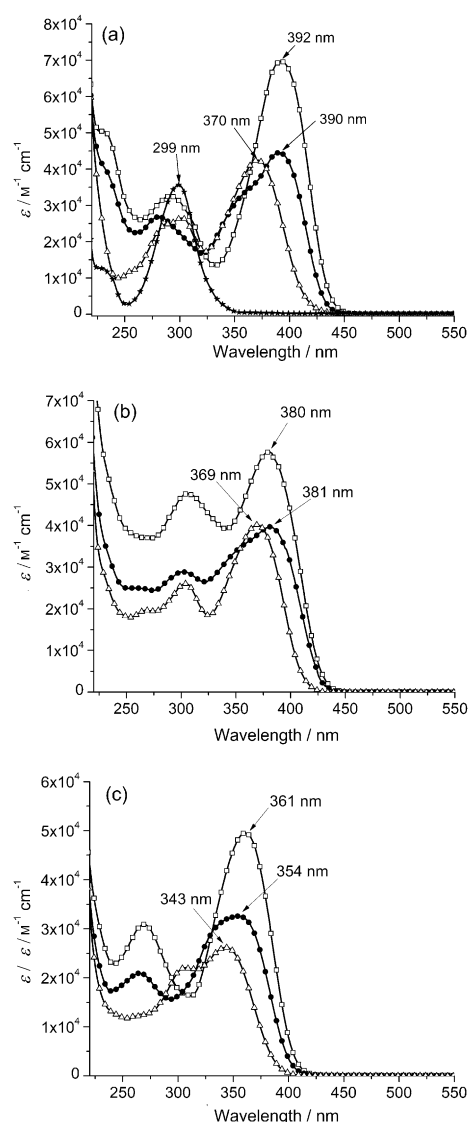


Figure 2. Absorption spectra of the TPA derivatives as solutions in THF ($c \sim 10^{-4}$ M). a) TPA (★), **1a** (□), **2a** (●), **3a** (Δ); b) **1b** (□), **2b** (●), **3b** (Δ); c) **1c** (□), **2c** (●), **3c** (Δ).

Table 2. Optical characteristics of the TPA derivatives.

| Compound | Absorption | | Fluorescence | | | | | | | | | | |
|-----------|---|---|---------------------------|-----------------|------------------------------------|----------------------------|---------------------------|-----------------|------------------------------------|----------------------------|---------------------------|-----------------|-------------------------------------|
| | Abs _{max} ^[a] [nm] | ϵ [M ⁻¹ cm ⁻¹] | Toluene solution | | | PS film (0.1 wt %) | | | | Neat film | | | |
| | | | Fl _{max} [nm] | Φ_F [%] | $\tau^{[b]}$ [ns] | Abs _{max} [nm] | Fl _{max} [nm] | Φ_F [%] | $\tau^{[b]}$ [ns] | Abs _{max} [nm] | Fl _{max} [nm] | Φ_F [%] | $\tau^{[b]}$ [ns] |
| 1a | 392 | 6.97×10^4 | 474 | 10 | 0.27 (81) 2.34 (19) | 401 | 461 | 54 | 1.33 (24) 2.28 (76) | 395 | 481 | 4 | 0.07 (84) 0.40 (13) 3.00 (3) |
| 2a | 390 | 4.45×10^4 | 469 | 5 | 0.20 (68) 0.21 (23) 2.1 (9) | 394 | 457 | 53 | 0.23 (3) 1.49 (30) 2.29 (67) | 396 | 480 | 8 | 0.08 (85) 0.35 (13) 2.68 (2) |
| 3a | 370 | 4.25×10^4 | 476 | 1 | 0.01 (74) 1.69 (5) 5.05 (21) | 380 | 453 | 45 | 0.55 (3) 1.92 (60) 2.87 (37) | 377 | 478 | 11 | 0.20 (56) 0.67 (41) 2.72 (3) |
| 1b | 380 | 5.77×10^4 | 462 | 13 | 0.08 (14) 0.51 (79) 2.19 (7) | 383 | 451 | 55 | 0.19 (3) 1.68 (65) 2.63 (32) | 382 | 480 | 6 | 0.10 (75) 0.46 (21) 2.82 (4) |
| 2b | 381 | 3.97×10^4 | 464 | 12 | 0.03 (21) 0.47 (72) 2.63 (7) | 382 | 451 | 62 | 0.80 (6) 1.97 (87) 3.39 (7) | 384 | 479 | 12 | 0.12 (70) 0.49 (26) 2.84 (4) |
| 3b | 369 | 4.02×10^4 | 477 | 5 | 0.17 (93) 4.73 (7) | 377 | 451 | 62 | 0.52 (2) 1.97 (68) 3.03 (30) | 374 | 479 | 18 | 0.19 (49) 0.80 (45) 3.40 (6) |
| 1c | 361 | 4.96×10^4 | 428 | 48 | 0.74 (22) 1.42 (78) | 367 | 424 | 58 | 1.89 (98) 10.2 (2) | 366 | 455 | 5 | 0.10 (62) 0.56 (30) 2.05 (8) |
| 2c | 354 | 3.26×10^4 | 424 | 44 | 1.25 | 357 | 422 | 63 | 1.06 (34) 1.80 (66) | 353 | 445 | 11 | 0.15 (55) 0.52 (39) 2.03 (6) |
| 3c | 343 | 2.62×10^4 | 424 | 16 | 0.61 (91) 4.55 (9) | 349 | 422 | 47 | 1.66 (87) 4.05 (13) | 349 | 446 | 23 | 0.30 (24) 1.06 (61) 4.08 (15) |

[a] Measured in solution in THF ($c \sim 10^{-4}$ M). [b] Fluorescence decay time constant estimated at Fl_{max}; the fractional contribution to the total fluorescence intensity [%] is given in parentheses.

The bathochromic shift of the absorption of **2a** and **3a** compared to that of TPA is attributed to extension of the core π -conjugated system by one and two diphenylethenyl units, respectively (Figure 2a). The maximum of the absorption spectra of **3a** is shifted by about 71 nm with respect to TPA and is located at $\lambda = 370$ nm. In line with expectations, the absorption of **2a** is shifted even more bathochromically, by about 91 nm relative to TPA. The additional diphenylethenyl fragment in **1a** has a very limited effect on the overall π -conjugated system of the molecule; the bathochromic shift on going from the di- to tri-substituted TPA derivative is very small (≈ 2 nm). However, absorption intensity increases quite noticeably. This indicates that the transition is accompanied by a larger change in the electronic charge distribution upon excitation. Addition of the methoxy groups in **1b** and **2b** (Figure 2b) generally yields smaller π -conjugated systems (hypsochromic shift of ≈ 10 nm) than **1a** and **2a**, which indicates that **1b** and **2b** adopt less planar configurations. As expected, substitution of the aromatic phenyl ring with a methyl group in compounds **1c–3c** (Figure 2c)

affects the overall π -conjugated system quite noticeably; a hypsochromic shift of around 30 nm relative to **1a–3a** is observed. However, TPA derivatives **1c** and **2c** are slightly less bulky than their analogues **1a** and **1b**, and **2a** and **2b**, respectively, therefore, it is easier for these molecules to adopt a more planar conformation. Addition of the third side arm in **1a** and **1b** had almost no effect on the position of the π - π^* transition band, however, in the case of **1c**, the bathochromic shift is more noticeable (≈ 7 nm).

The propeller-like structure of the TPA core with highly twisted ($\approx 50^\circ$) phenyl rings around the C–N bonds implies effective C–N stretching vibrations and phenyl torsions, which greatly affects n - π conjugation and, thus, the spectroscopic properties of TPA and the TPA-derived compounds.^[14] On the other hand, the nonplanar TPA geometry predefines intricate molecular packing in the solid state, which results in nontrivial optical and charge-transport properties of the TPA compounds. Generally, the attachment of phenylethenyl side arms to the phenyl groups of the TPA core is expected to hinder phenyl vibrations/torsions

and, consequently, by systematic variation of the number and type of the side arms, tune the optical and charge-transport properties of the compounds. To differentiate between the intramolecular motions and intermolecular effects, the TPA compounds were investigated in different media (solution, rigid polymer matrix, and neat film). Figure 3 displays

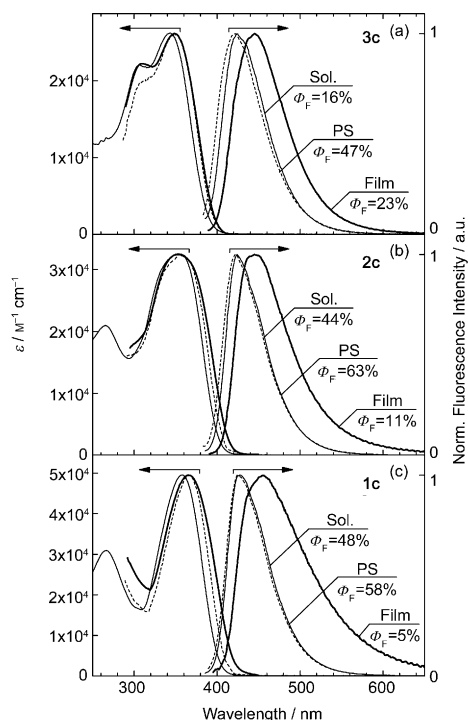


Figure 3. Absorption and fluorescence spectra of TPA derivatives a) **3c**, b) **2c**, and c) **1c** that contain a varied number of phenylethenyl side arms as solutions in toluene ($c \sim 10^{-5}$ M) [—], as PS matrixes ($c = 0.1$ wt %) [---], and as neat films (—). Φ_F values indicated. Absorption spectra of the compounds in PS matrixes and neat films are normalized to the spectra of the compounds in solution, which are presented in absolute values.

the absorption and fluorescence spectra of the structurally modified TPA derivatives with one, two, and three phenylethenyl (stilbene-like) side arms. The details of the optical properties of the compounds are summarized in Table 2.

In contrast to the absorption spectra dynamics, the fluorescence-band maximum of the TPA derivatives **1c–3c** is found to be independent of the number of stilbene-like side arms ($\lambda \approx 426$ nm). Nearly identical spectra of the compounds in solution in toluene and those of the compounds dispersed in polystyrene (PS) matrixes point out that planarization of the noninteracting molecules **1c–3c** is unlikely in solution in the excited state.^[15] The stilbene-like side arms are twisted out of the plane of the C–N bonds (like the phenyl moieties in the propeller-shaped unsubstituted TPA molecule) and the TPA derivatives can undergo planarization in solution, which is suppressed in a rigid polymer matrix. Because the planarization is accompanied by an extension of the π -conjugated system, experimentally evi-

denced by a spectral shift to longer wavelengths, the absence of this shift in the fluorescence spectra of the compounds in solution in toluene indicates that planarization is improbable. A similar argument rules out possible alteration of the electron–vibron coupling with an increasing number of stilbene-like side arms.

In spite of the similar fluorescence spectra, fluorescence quantum yield (Φ_F) of the TPA compounds in dilute solutions increases with the number of side arms from 16% for compound **3c** with one side arm to 48% for compound **1c** with three side arms (Figure 4a). Evidently, the enhance-

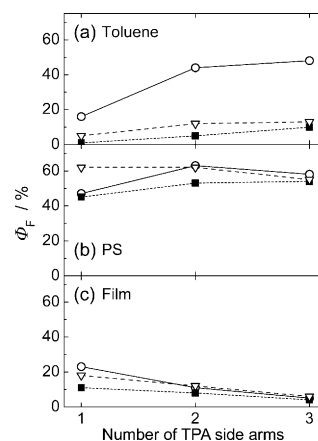


Figure 4. Φ_F of the TPA derivatives versus number of TPA side arms a) as a solution in toluene ($c \sim 10^{-5}$ M), b) as PS matrixes ($c = 0.1$ wt %), and c) as neat films. **1a–3a** (■); **1b–3b** (▽); **1c–3c** (○).

ment of Φ_F is invoked by hindrance of the vibrations/torsions of the phenyl groups of the TPA core by the side arms and, thus, the torsion-activated nonradiative relaxation pathway is considerably reduced. This result is confirmed by the high value of Φ_F obtained for compounds **1c–3c** in rigid PS matrixes, in which intramolecular vibrational/torsional motions of the phenyl groups are suppressed irrespective of the presence of adjoining side arms (Figure 4b). Consequently, Φ_F varies insignificantly (47–63%) with respect to the number of stilbene-like side arms attached. Note, however, that at least one stilbene-like side arm is required to attain such high Φ_F values; the unsubstituted TPA molecule incorporated in a PS matrix exhibits a Φ_F of only around 4%.

Fluorescence spectra of the neat films of the TPA derivatives **1c–3c** are broadened and redshifted relative to those of the compounds in solution in toluene, which corresponds with enhanced intermolecular interactions in the solid state (Figure 4). These features are most pronounced for compound **1c**, which bears three side arms; this suggests that stilbene-like side arms play a major role in the molecular packing that leads to increased intermolecular interaction. Unlike in solution, an increase in the number of side arms diminishes Φ_F values in the TPA neat films (Figure 4c). The Φ_F values continuously decrease from 23% for compound **3c** with one side arm to 5% for compound **1c** with three side arms. Intuitively, the incorporation of more branches

into the TPA molecule is supposed to prevent molecule aggregation in the solid state and, thus, result in enhanced Φ_F . However, in this particular case, the stilbene-like side arms most likely arrange in a densely overlapping pattern, which facilitates excitation migration and migration-induced relaxation at nonradiative decay sites. Similar trends in the optical properties versus the number of side arms were also observed for the rest of the TPA compound series **1a–3a** and **1b–3b**.

Introduction of a second phenyl group into the stilbene-like side arms (compounds **1a–3a**) resulted in redshifted (by 20–50 nm) absorption and fluorescence bands. Similar behavior was also observed in the presence of diphenylethenyl side arms with methoxy substituents (compounds **1b–3b**). Although the extended conjugation conditioned nearly two-fold enhanced absorbance, the additional phenyl moiety detrimentally affected the Φ_F of **1a–3a** and **1b–3b** in solution in toluene (Figure 4a). For the materials with one side arm, Φ_F dropped from 16% (**3c**) to 1 and 5% for **3a** and **3b**, respectively (Figure 5). This drastic reduction of Φ_F is attributed to induced steric hindrance from the second phenyl

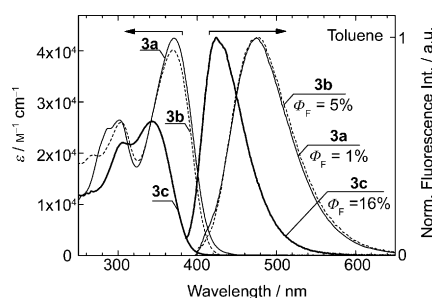


Figure 5. Absorption and fluorescence spectra of TPA derivatives with one side arm in solution in toluene ($c \sim 10^{-5}$ M). **3a** (—), **3b** (---), and **3c** (···); Φ_F values indicated.

group, which activates phenyl vibrations/torsions and, thus, promotes radiationless decay.^[16] Note that the reduction of Φ_F for compounds **1b–3b** is smaller than for **1a–3a** because the phenyl motions are somewhat impeded by the presence of the methoxy moieties. Likewise, for **1c–3c**, an increased number of side arms led to increased Φ_F (Figure 4a) and caused greater redshift of the absorption bands relative to the fluorescence bands. However, in contrast to compounds **1c–3c**, the fluorescence spectra of compounds **1a–3a** and **1b–3b** dispersed in PS matrixes are blueshifted relative to the spectra of the compounds in solution in toluene (see Table 2). This result illustrates that the additional phenyl group in the diphenylethenyl side arms provokes planarization of the molecules in the excited state.^[15] Incorporation of compounds **1a–3a** and **1b–3b** in PS matrixes strongly diminished the nonradiative relaxation rate by suppressing phenyl torsions and, therefore, boosted Φ_F up to 45–54 and 55–62%, respectively. These Φ_F values are very similar to those obtained for compounds **1c–3c** with stilbene-like side

arms and are roughly independent of the number of side arms attached (Figure 4b).

Fluorescence spectra of the neat films of **1a–3a** and **1b–3b** were found to be slightly redshifted relative to the spectra of the same compounds in toluene solution or PS matrixes. However, the spectral shape remained unchanged and contained no traces of vibronic structure, which verified an amorphous character of the films formed. A monotonous decrease of FF (from 11 to 4%, from 18 to 6%, and from 23 to 5% in the neat films of **1a–3a**, **1b–3b**, and **1c–3c**, respectively) with an increasing number of side arms highlighted the key role of the diphenylethenyl fragments in exciton migration and migration-induced nonradiative deactivation at quenching sites (distortions, defects, etc.; Figure 4c).

Generally, the fluorescence transients of the TPA derivatives **1c–3c** (Figure 6), as well as of **1a–3a** and **1b–3b**, demonstrate multi-exponential decays that result from various molecular conformations, which are feasible due to the

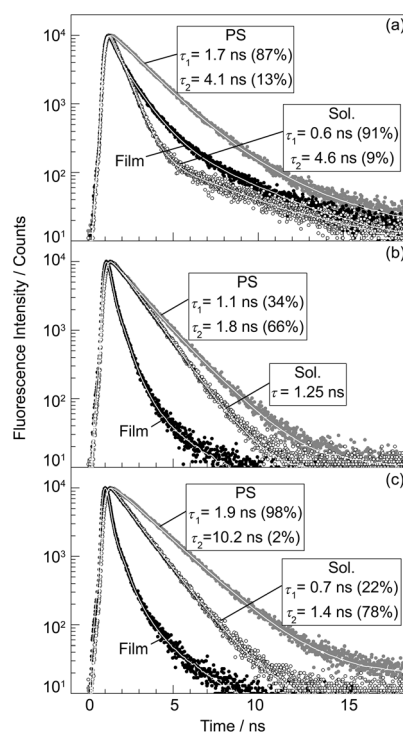


Figure 6. Fluorescence transients of TPA derivatives a) **3c**, b) **2c**, and c) **1c** that contain a varied number of phenylethenyl side arms as a solution in toluene ($c \sim 10^{-5}$ M; empty circles), as PS matrixes ($c = 0.1$ wt %; grey filled circles), and as neat films (black filled circles). Lines mark single and double exponential fits to the experimental data. Fluorescence decay time constants indicated.

labile phenyl groups. For a quantitative comparison of the decay rates of multi-exponential transients, the dominant decay-time component (τ) with the largest fractional intensity was used. The transients reflected fairly well the tendencies of Φ_F evaluated in different media (dilute solution in toluene, PS film, or neat film) as a function of the number

and type of phenylethenyl side arms. An increase in the number of side arms caused prolonged τ in solution media, in agreement with the enhanced Φ_F values obtained, which implies suppression of the phenyl torsions in the TPA core. The increase of τ with the number of side arms was observed irrespectively of the type of phenylethenyl side arms attached, though the presence of a second phenyl group in the diphenylethenyl moieties (compounds **1a–3a** and **1b–3b**) strongly activated phenyl torsions and, thus, torsion-induced nonradiative decay, thereby τ was reduced considerably. The reduction of τ from 0.6 ns (**3c**) to 0.1 ns (**3a**) for compounds that contain one side arm is evidenced in Figure 7. Initial fluorescence decay of compounds **3a** and **3b**, which

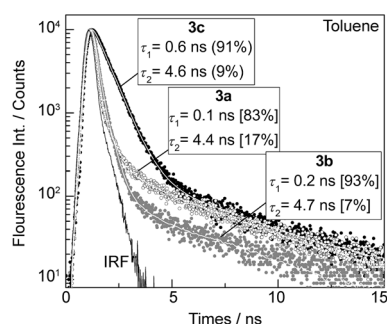


Figure 7. Fluorescence transients of TPA derivatives **3a** (empty circles), **3b** (filled grey circles), and **3c** (filled black circles) with a single side arm ($c \sim 10^{-5}$ M in toluene). IRF=instrument-response function. Lines mark double exponential fits to the experimental data. Fluorescence decay time constants indicated.

bear sterically hindered phenyl groups, is so rapid that it approaches the temporal resolution (0.07 ns) of our experimental setup. On another hand, suppression of phenyl torsions by incorporation of the TPA derivatives in rigid PS matrixes significantly increases τ up to 1.7–2.4 ns, regardless of the number and type of side arms used (see Figure 6 and Table 2). Again, this behavior perfectly correlates with the enhanced Φ_F observed upon incorporation of the derivatives in PS matrixes and also with the independence of this enhancement on the type and number of phenylethenyl side arms (Figure 4b).

In the neat films of the TPA compounds that contain both two and three side arms fluorescence transients become very fast (they are close to the instrument-response function (IRF) of the experimental setup). As found in dilute (0.1 wt %) PS matrixes, phenyl torsions are severely inhibited in the neat films of the compounds, however, as opposed to the polymer matrix, the condensed phase enables excitation migration, which facilitates excitation quenching at non-radiative decay sites. This is the main cause of the fast excited-state decay observed in the neat film samples. Moreover, a general tendency for τ to decrease with an increase in the number of phenylethenyl side arms, irrespectively of their type, indicates a more favorable arrangement of the molecules with more arms that result in more efficient excitation migration. The latter result is in agreement with the de-

crease of Φ_F when the compound contains a greater number of side arms, observed in the neat films due to enhanced excitation migration (Figure 4c).

From a practical and fundamental point of view it is important to investigate fluorescence concentration quenching of the TPA derivatives and elucidate the impact of the number of phenylethenyl side arms on the quenching. Concentration quenching of the compounds was explored by dispersion in a rigid transparent PS matrix and evaluating Φ_F dynamics versus concentration in the range $c = 0.1$ –100 wt % (Figure 8). At concentrations up to 1 wt %, the quenching

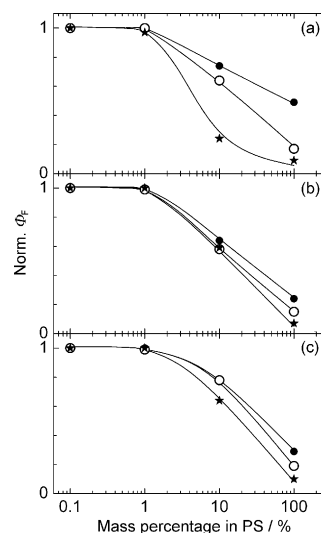


Figure 8. Normalized Φ_F values of the TPA derivatives as a function of concentration in PS matrix. a) **1c** (★), **2c** (○), **3c** (●); b) **1a** (★), **2a** (○), **3a** (●); c) **1b** (★), **2b** (○), **3b** (●).

was negligible, whereas a further increase of the concentration lowered the Φ_F by up to ten times. Clearly, the quenching became more pronounced with an increased number of phenylethenyl side arms, regardless of the type of side arm linked to the TPA core. These findings support the data that demonstrate the most remarkable drop of Φ_F and τ in the neat films of TPA compounds that feature the largest number of side arms (**1a–1c**), and proves a significance of the phenylethenyl side arms in the enhancement of exciton migration.

Charge-transport properties: Charge-transport properties of the synthesized TPA derivatives **1–3** were studied by the xerographic time-of-flight (XTOF) technique^[17] (Figure 9). The values of the parameters that define charge mobility [zero field mobility (μ_0), Poole–Frenkel parameter (α)] and the mobility (μ_h) at the electric field strength of 6.4×10^5 V cm⁻¹ are given in Table 3 for compounds **1–3**.

The room temperature hole drift mobility of the as-spun film of the trisubstituted TPA derivative **1a** was $\mu_h = 0.017$ cm² V⁻¹ s⁻¹ at strong electric fields and is approximately four-times higher than that of the monosubstituted analogue **3a**. Compound **2a** demonstrated similar performance

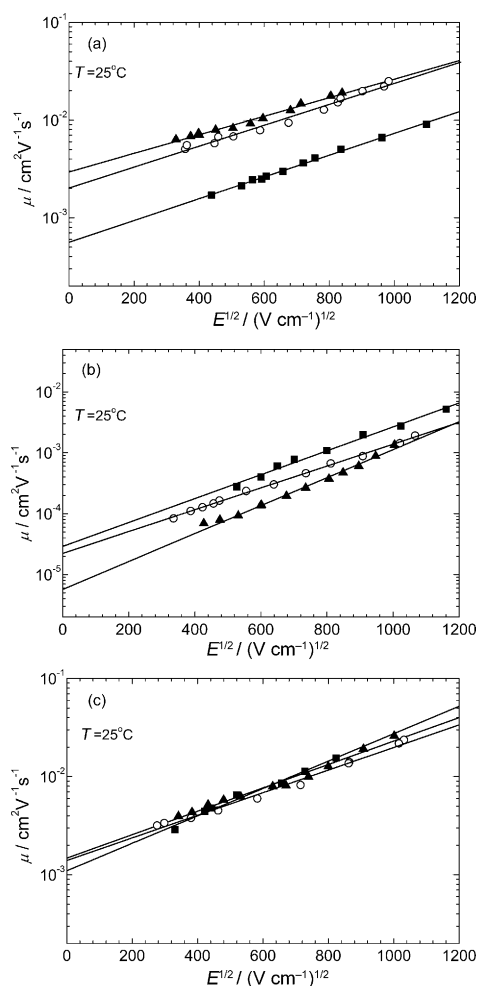


Figure 9. Electric-field dependencies of the hole drift mobilities (μ) in charge-transport layers of TPA derivatives. a) **1a** (▲), **2a** (○), **3a** (■); b) **1b** (▲), **2b** (○), **3b** (■); c) **1c** (▲), **2c** (○), **3c** (■).

to **1a** with μ_h as high as $0.014 \text{ cm}^2 \text{ V}^{-1} \text{ s}^{-1}$. Hole mobility in methoxy-substituted HTMs **1b** and **2b** was two orders of magnitude lower than in the corresponding unsubstituted analogues **1a** and **2a**. Most likely the manner in which molecules organize in the layer is altered unfavorably by addition

of the methoxy groups. Even though compounds **1c** and **2c** possess the smallest π -conjugated systems of all the HTMs investigated, a streamlined structure, which is less bulky than **1a** and **2a** or **1b** and **2b**, allows easier arrangement of the molecules into conformations more favorable for charge transport. As a result, hole mobilities of **1c** and **2c** reach $\mu_h = 0.013 \text{ cm}^2 \text{ V}^{-1} \text{ s}^{-1}$ and are very similar to those demonstrated by **1a** and **2a**.

It has been recognized that solution-processed materials offer a better ease of processing than vacuum-deposited materials, but generally have lower carrier mobility. The lower mobility is generally attributed to the lower structural order that reduces intermolecular π -orbital overlap. However, compared with other low-molecular-weight triarylamines (Table 4), diphenylethenyl-substituted TPA derivatives **1a**, **1c**, **2a**, and **2c** demonstrate relatively high hole drift mobility that is an order of magnitude higher than very well known HTM, *N,N'*-bis(3-methylphenyl)-*N,N'*-diphenylbenzidine (TPD). Note that these results were obtained from solution-processed films, whereas the majority of the best-performing low-molecular-weight triarylamines were vacuum deposited.

The electronic properties of molecular-transport materials depend on the manner in which the molecules are organized in the solid state.^[19] In particular, π -stacking, although not a guarantee of good wavefunction overlap,^[20] is a feature of many high-mobility materials.^[21]

Analysis of the optical properties of the investigated materials indicates that side arms play a major role in the molecular packing that leads to increased intermolecular interaction. Intuitively, the incorporation of more branches into the TPA molecule is supposed to prevent molecule aggregation in the solid state and, thus, result in enhanced Φ_F , however, in this particular case, the stilbene-like side arms most likely arrange in a densely overlapping pattern.

Energy spectra: To elucidate the energetic conditions for energy and electron transfer in dilute solutions, the E_{HOMO} and E_{LUMO} values were determined by cyclic voltammetry (CV) [Table 3]. These values do not represent any absolute solid-state or gas-phase ionization potentials, but can be

Table 3. E_{HOMO} , E_{LUMO} , I_p , bandgap energies, and hole mobility data for **1–3**.^[a]

| Compound | $E_g^{\text{opt}}[\text{b}]$ [eV] | E_{HOMO} [V vs. NHE] | $E_{\text{LUMO}}[\text{c}]$ [V vs. NHE] | $I_p[\text{d}]$ [eV] | d [μm] | $\mu_0^{\text{[e]}}$ [$\text{cm}^2 \text{ V}^{-1} \text{ s}^{-1}$] | $\mu_h^{\text{[f]}}$ [$\text{cm}^2 \text{ V}^{-1} \text{ s}^{-1}$] | α [$\text{cm}^{1/2} \text{ V}^{-1/2}$] |
|-----------|--------------------------------------|----------------------------------|--|-------------------------|--------------------------|---|---|--|
| 1a | 2.76 | 0.92 | −1.84 | 5.41 | 6.3 | 3×10^{-3} | 0.017 | 0.0022 |
| 2a | 2.78 | 0.92 | −1.86 | 5.35 | 2.9 | 2×10^{-3} | 0.014 | 0.0025 |
| 3a | 2.88 | 0.94 | −1.94 | 5.43 | 4.9 | 5.6×10^{-4} | 4.3×10^{-4} | 0.0045 |
| 1b | 2.81 | 0.86 | −1.95 | 5.27 | 3.4 | 5.6×10^{-6} | 3.9×10^{-4} | 0.0053 |
| 2b | 2.82 | 0.84 | −1.98 | 5.23 | 4.8 | 2.2×10^{-5} | 6×10^{-4} | 0.0041 |
| 3b | 2.92 | 0.85 | −2.07 | 5.35 | 2.3 | 3×10^{-5} | 1.1×10^{-3} | 0.0045 |
| 1c | 2.97 | 0.93 | −2.04 | 5.45 | 6 | 1.5×10^{-3} | 0.013 | 0.0027 |
| 2c | 2.98 | 0.93 | −2.05 | 5.47 | 6.4 | 1.4×10^{-3} | 0.012 | 0.0027 |
| 3c | 3.06 | 0.94 | −2.12 | 5.45 | 6.3 | 1.1×10^{-3} | 0.014 | 0.0032 |

[a] The CV measurements were carried out at a glassy carbon electrode in CH_2Cl_2 that contained 0.1 M tetrabutylammonium hexafluorophosphate as the electrolyte and Ag/AgNO_3 as the reference electrode. Each measurement was calibrated with ferrocene (Fc). Potentials measured versus Fc^+/Fc were converted to the normal hydrogen electrode (NHE) by addition of +0.63 V. [b] The optical bandgaps (E_g^{opt}) were estimated from the edges of the electronic absorption spectra. [c] $E_{\text{LUMO}} = E_{\text{HOMO}} - E_g^{\text{opt}}$. [d] Ionization potential was measured by the photoemission-in-air method from films. [e] Mobility value at zero field strength. [f] Mobility value at $6.4 \times 10^5 \text{ V cm}^{-1}$ field strength.

used to compare different compounds relative to one another. The cyclic voltammograms of the synthesized compounds in dichloromethane show one quasireversible oxidation couple and no reduction waves (see the Supporting Information; Figure S1 and Table S1).

The additional side arms in **1a** and **2a** did not influence energy levels much; the energy levels remained quite similar to those demonstrated by monosubstituted TPA **3a**, and only a very slight decrease in E_{HOMO} was observed. Very similar E_{HOMO} values were

also determined for **1c–3c**, although substitution of the phenyl group with a methyl group decreased E_{LUMO} by about 0.2 V. The methoxy groups in **1b–3b** promote a decrease of E_{HOMO} by about 0.1 V relative to **1a–3a**. However, as with all other examples, there is almost no difference between the E_{HOMO} levels in mono-, di-, and trisubstituted TPA derivatives. Additional phenylethenyl groups have a more substantial effect on E_{LUMO} , which increases by approximately 0.1 V with addition of the second fragment.

When an organic material is considered for use in optoelectronic applications it is important to have an understanding of its solid-state ionization potentials (I_p). This understanding can help with identification of suitable partner organic transport materials and inorganic electrode materials. The ionization potential was measured by the ‘electron photoemission in air’ method (Figure 10) and the results are presented in Table 3; the measurement error is evaluated as 0.03 eV.^[22]

Usually the photoemission experiments are carried out in a vacuum; more specifically, high vacuum is one of the main requirements for these measurements. If the vacuum is not high enough sample surface oxidation and gas adsorption influence the measurements. In our case, however, the organic materials investigated are stable enough to oxygen that the measurements may be carried out in the air. The measured I_p values are about 0.3 eV higher than the E_{HOMO} levels found in the CV experiments. The difference may result from different measurement techniques and conditions (solution samples for

Table 4. Hole mobility of various low-molecular-weight triarylamines.

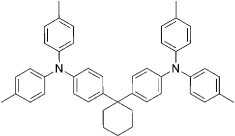
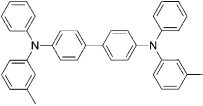
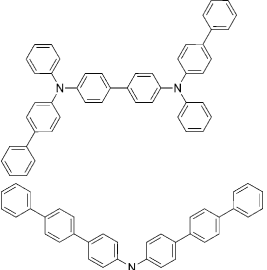
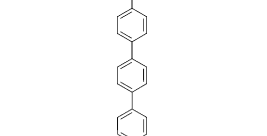
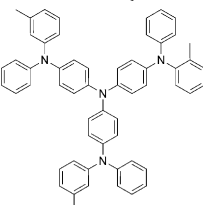
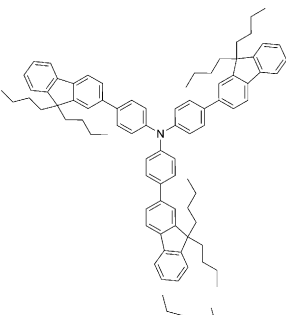
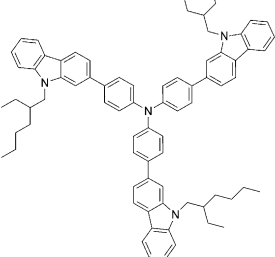
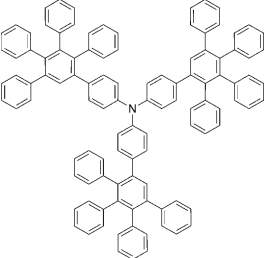
| Compound | μ [cm ² V ⁻¹ s ⁻¹] | Layer-formation method | Reference |
|---|---|------------------------|-----------|
|  | 1×10^{-2} | vacuum deposition | [7] |
|  | 1.1×10^{-3} | vacuum deposition | [18a] |
|  | 1×10^{-3} | vacuum deposition | [18b] |
|  | 6.9×10^{-3} | vacuum deposition | [18c] |
|  | 3×10^{-5} | vacuum deposition | [18d] |
|  | 1×10^{-4} | spin coating | [9] |
|  | 3×10^{-4} | spin coating | [9] |

Table 4. (Continued)

| Compound | μ [cm ² V ⁻¹ s ⁻¹] | Layer-formation method | Reference |
|---|---|------------------------|-----------|
|  | 5×10^{-5} | vacuum deposition | [18e] |

CV and solid-film samples for the photoemission method). Compounds **1c–3c** demonstrate the highest I_p values of all three groups investigated. Interestingly, **1a–3a** have similar E_{HOMO} levels in solution, however, their ionization potentials are slightly lower. Most likely this is caused by differences in the way these molecules pack in the solid state. The presence of methoxy groups in **1b–3b** lowers the I_p by about 0.1 eV relative to **1a–3a**.

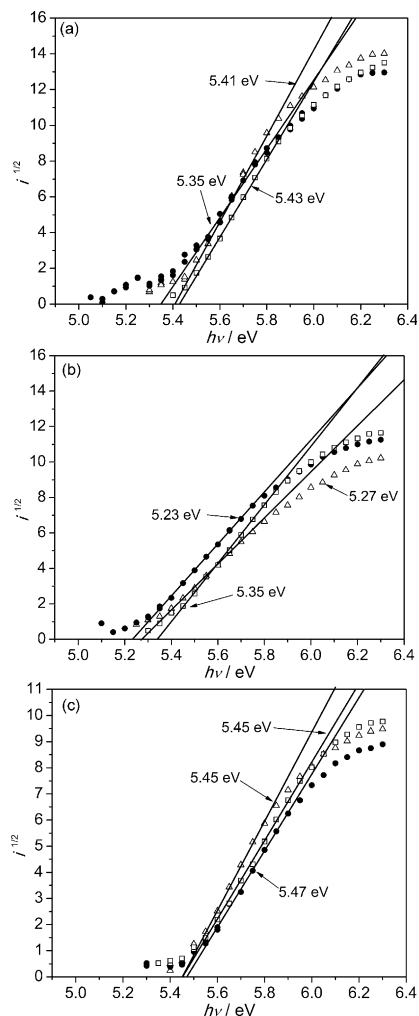


Figure 10. Photoemission-in-air spectra of **1–3**. a) **1a** (Δ), **2a** (\bullet), **3a** (\square); b) **1b** (Δ), **2b** (\bullet), **3b** (\square); c) **1c** (Δ), **2c** (\circ), **3c** (\blacksquare)

Organic photoreceptor device fabrication and parameters:

HTMs with three side arms, **1a–c**, were used in the construction of organic photoreceptor devices (Figure 11). The devices consisted of a conducting Al layer, 0.5 μm thick charge-generation layer (CGL) composed of a 2:1 mass proportion of titanyl phthalocyanine and polyvinyl butyral BX-1, and charge-transporting layer (CTL), which consisted of a 1:1

mass proportion mixtures of the transporting material and polycarbonate Z-200 (PC-Z).

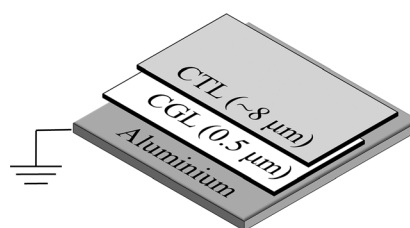


Figure 11. Structure of the organic photoreceptor devices.

Characteristics of the devices constructed from investigated materials **1a–1c** were compared with well-known and efficient HTM, TPD (Table 5). Photosensitivity (S) of the synthesized TPA derivatives with phenylethenyl side arms is very similar or better than that of TPD. Relative residual potential (U_R/U_0) is lowest for **1a**, whereas the device created with **1b** demonstrates similar results to one constructed with TPD. In the case of **1c**, despite higher mobility than **1b**, the remaining residual potential is larger; this could likely be attributed to a higher rate of trap formation. Figure 12 shows the spectral distribution of the photosensitivity of an organic photoreceptor constructed from **1b** or TPD. Both compositions exhibit good xerographic photosensitivity across most of the visible-light region of the spectrum, although somewhat better results are observed for **1b**.

Similar tendencies to those observed with residual potential are noted on analysis of the potential decay curves after illumination with a $\lambda=780$ nm light pulse (Figure 13). The potential drops rapidly in the devices that contain HTMs with diphenylethenyl- and methoxy-substituted side arms (**1a** and **1b**), whereas **1c** performs slightly worse for the same reasons explained above.

Despite considerable reduction of the HTM concentration in the CTL layer, the hole mobility remains very good. In all cases it is better than the μ_h of TPD under identical conditions (Figure 14, Table 5). The best results ($\mu_h=7.5 \times 10^{-4}$ cm²V⁻¹s⁻¹ at strong electric fields) are observed for the device constructed from TPA derivative **1a** with three diphenylethenyl side arms.

Table 5. Characteristics of the organic photoreceptor devices that contain **1a–c**.

| Compound | d [μm] | U_0 [V] | $S^{[a]}$ [m^2J^{-1}] | U_R [V] | U_R/U_0 | $t_{1/2}$ [s] | $\mu_0^{[b]}$ [$\text{cm}^2\text{V}^{-1}\text{s}^{-1}$] | $\mu^{[c]}$ [$\text{cm}^2\text{V}^{-1}\text{s}^{-1}$] | α [$\text{cm}^{1/2}\text{V}^{-1/2}$] |
|-----------|--------------------------|--------------|--|--------------|-----------|------------------|--|--|--|
| 1a | 7.2 | −348 | 478 | −6.6 | 0.019 | 0.082 | 1.4×10^{-5} | 7.5×10^{-4} | 0.005 |
| 1b | 9.9 | −478 | 396 | −14.3 | 0.03 | 0.094 | 7.2×10^{-7} | 1.8×10^{-4} | 0.0069 |
| 1c | 7.5 | −495 | 384 | −30 | 0.061 | 0.104 | 3.1×10^{-5} | 5.3×10^{-4} | 0.0035 |
| TPD | 7.2 | −461 | 368 | −13.2 | 0.029 | 0.102 | 4.6×10^{-6} | 1.3×10^{-4} | 0.0042 |

[a] $\lambda = 780$ nm. [b] Mobility value at zero field strength. [c] Mobility value at 6.4×10^5 V cm^{-1} field strength.

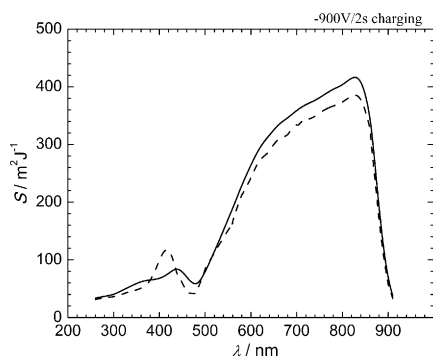


Figure 12. Electrophotographic spectral photosensitivity of **1b** (—) and TPD (----).

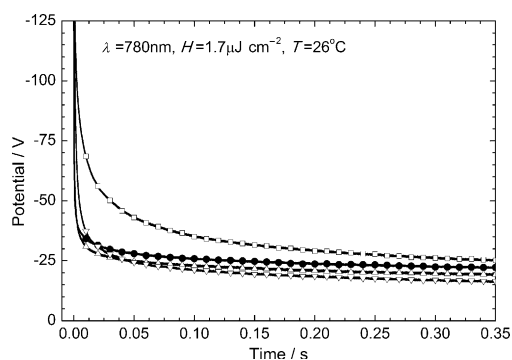


Figure 13. The potential decay curves of the photoreceptor devices after 1 μs of illumination with a xenon flash lamp ($\lambda = 780$ nm light pulse). The exposition $H = 1.7 \mu\text{J cm}^{-2}$. Negative initial potential: TPD (●) -431 V, **1a** (Δ) -383 V, **1b** (∇) -443 V, **1c** (\square) -438 V.

Conclusion

We have demonstrated a simple one-step synthesis to obtain solution processable star-shaped charge-transport materials with a TPA core and a varied number of different phenylethenyl side arms from commercially available and relatively inexpensive starting materials. Substitutions in the phenylethenyl fragment could noticeably influence the HTMs T_g values and tendency to crystallize. By structural modification of the side arms, the size of the π -conjugated system, energy levels, and the way the molecules pack in the solid state can also be significantly influenced. Optical measurements revealed that an increase in the number of side arms effectively suppressed intramolecular motions of the TPA

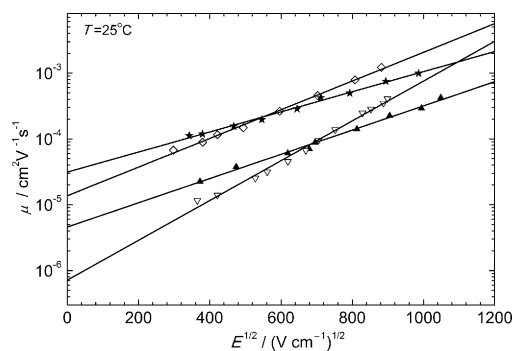


Figure 14. The mobility field dependencies of the electrophotographic samples. TPD (\blacktriangle), **1a** (\diamond), **1b** (∇), **1c** (\blackstar).

core in solution, whereas in the solid state it facilitated exciton migration through the dense side-arm network formed. In turn, this dense network enables charges to move more rapidly through the HTM layer and results in very good charge drift mobilities of up to $0.017 \text{ cm}^2 \text{V}^{-1} \text{s}^{-1}$ at strong electric fields. Organic photoreceptor devices were constructed using HTMs **1a–1c**. The test results demonstrate that these materials outperform well-known HTM, TPD. Due to their low T_g values, **1c** and **2c** could be used as HTMs in solid-state dye-sensitized solar cells, in which good pore filling is needed. Out of the HTMs investigated, compounds **1a** and **1c** are especially promising candidates for practical applications because they can be handled in air, require no high-temperature annealing steps, can be solution deposited, possess comparatively high mobility, and can be synthesized in one step from commercially available and cheap starting material TPA.

Experimental Section

General: Chemicals were purchased from Sigma–Aldrich and TCI Europe and used as received without further purification. Compounds **1a–3a**^[10] and bis(4-methoxyphenyl)acetaldehyde^[23] were synthesized by procedures reported previously. ^1H and ^{13}C NMR spectra were recorded on a Varian Unity Inova (300 MHz) spectrometer at room temperature with chemical shifts (δ) reported in ppm and TMS ($\delta = 0$ ppm) as an internal standard. The reactions were monitored by TLC on ALUGRAM SIL G/UV254 plates and plates were developed with I_2 or viewed under UV light. Silica gel (grade 9385, 230–400 mesh, 60 \AA , Aldrich) was used for column chromatography. Elemental analysis was performed with an Exeter Analytical CE-440 Elemental instrument. DSC measurements were performed with a Q10 calorimeter (TA Instruments) at a scan rate

of 10 K min⁻¹ under a nitrogen atmosphere. The T_g values for the investigated compounds were determined during the second heating scan.

Optical measurements: Absorption spectra of the dilute solutions in THF were recorded on a UV/Vis-NIR spectrophotometer, Lambda 950 (Perkin-Elmer). Fluorescence of the investigated compounds as PS- or neat films was initiated by a light-emitting diode ($\lambda=365$ nm; Nichia NSHU590-B) and measured by using a back-thinned charge-coupled device (CCD) spectrophotometer PMA-11 (Hamamatsu). For these measurements, a dilute solution of the required compound was prepared by dissolution in spectral-grade toluene ($c=1\times 10^{-5}$ M). PS films with concentrations that ranged from 0.1–100 wt % were prepared by mixing the dissolved compound with a solution of PS in toluene at the appropriate ratio and casting the solutions on quartz substrates under ambient conditions. Drop casting from solutions in toluene (1×10^{-3} M) was also employed to prepare neat films of the compounds. The Φ_F of the solutions were estimated by comparison of the wavelength-integrated photoluminescence (PL) intensity of the compound solutions to that of quinine sulfate in a 0.1 M aqueous solution of H₂SO₄ ($\Phi_F=53\pm 2.3$) as a reference.^[24] Optical densities of the reference and sample solutions were kept below 0.05 to avoid reabsorption effects. Estimated quantum yields of the compound solutions were verified by using the integrated-sphere method.^[25] An integrating sphere (Sphere Optics) coupled to the CCD spectrometer by optical fiber was also employed to measure the Φ_F of the neat and PS films. Fluorescence transients of the samples were measured by using a time-correlated single-photon-counting system PicoHarp 300 (PicoQuant), which utilizes a semiconductor diode laser (repetition rate = 1 MHz, pulse duration = 70 ps, $\lambda_{\text{emission}}=375$ nm) as an excitation source.

CV measurements: The electrochemical studies were carried out by a three-electrode assembly cell from Bio-Logic SAS and a micro-AUTO-LAB Type III potentiostat-galvanostat. The measurements were carried out with a glassy carbon electrode in dichloromethane solutions that contained tetrabutylammonium hexafluorophosphate (0.1 M) as the electrolyte, Ag/AgNO₃ as the reference electrode, and a Pt wire counter electrode. Each measurement was calibrated with ferrocene (Fc). Oxidation potentials were obtained as an average value between each anodic (pa) and corresponding cathodic potential (pc) [$E_{1/2}^{\text{red/ox}}=1/2(E_{\text{pc}}+E_{\text{pa}})$]. The optical bandgaps (E_g^{opt} [eV]) were estimated from the edges of the electronic absorption spectra, E_{LUMO} values by using the equation $E_{\text{LUMO}}=E_{\text{HOMO}}-E_g$.

Ionization-potential measurements: The ionization potential (I_p) of the layers of the synthesized compounds was measured by electron photoemission in air.^[22] The samples were prepared by dissolution in CHCl₃ and the solutions were coated on Al plates pre-coated with approximately 0.5 μm thickness of a methylmethacrylate and methacrylic acid copolymer adhesive layer. The thickness of the transporting material layer was 0.5–1 μm . The organic materials investigated are stable enough to oxygen that the measurements may be carried out in the presence of air. The samples were illuminated with monochromatic light from a quartz monochromator fitted with a deuterium lamp. The power of the incident light beam was $2\text{--}5\times 10^{-8}$ W. A negative voltage (–300 V) was supplied to the sample substrate. The counter electrode with a 4.5×15 mm² slit for illumination was placed 8 mm from the sample surface. The counter electrode was connected to the input of the BK2–16 type electrometer, working in the open input regime, for the photocurrent measurement. A 10^{-15} – 10^{-12} A photocurrent (I) flowed in the circuit under illumination. The value of I is strongly dependent on the incident-light photon energy ($h\nu$). The dependence $I^{0.5}$ on incident-light quanta energy $h\nu$ was plotted from the experiment results. Usually the dependence of I on the incident light quantum energy is described well by the linear relationship between $I^{0.5}$ and $h\nu$ near the threshold.^[22b,c] The linear part of this dependence was extrapolated to the $h\nu$ axis and the I_p value was determined as the photon energy at the interception point.

Hole-drift-mobility measurements: The samples for the hole-drift-mobility measurements were prepared by spin coating solutions of the synthesized compounds in toluene onto PS films with a conductive Al layer. The layer thickness was in the range 5–10 μm . The hole drift mobility was measured by XTOF.^[17] An electric field was created by positive corona charging. The charge carriers were generated at the layer surface

by illumination with pulses of a nitrogen laser (pulse duration = 2 ns, $\lambda=337$ nm). The layer surface potential decrease as a result of pulse illumination was up to 1–5 % of the initial potential before illumination. The capacitance probe that was connected to the wide-frequency band electrometer measured the speed of the surface potential decrease (dU/dt). The transit time (t_t) was determined by the kink on the curve of the dU/dt transient on a linear or double logarithmic scale. The drift mobility was calculated by the formula $\mu=d^2/U_0t_t$ (d is the layer thickness, U_0 is the surface potential at the moment of illumination).

Construction of the organic photoreceptor: Hole-transporting material TPD was purchased from Sigma–Aldrich. The samples of electrophotographic layers were prepared on PS film substrates with a conducting Al layer and CGL (0.5 μm thickness) composed of 2:1 mass proportion composition of titanyl phthalocyanine ELA7051 (H. W. Sands Co.) and polyvinyl butyral BX-1 (Sekisui). The HTM layers were coated by the doctor-blade method from the 1:1 mass proportion mixtures of the transporting materials and polycarbonate Z-200 (Mitsubishi Gas Chemical Co.) dissolved in THF. After coating, the samples were heated at 80 °C for 1 h to dry. The thickness of the transporting layers was approximately 8 μm . The electrophotographic parameters of the samples were measured as described in the literature.^[26]

General synthetic procedure: The appropriate triarylamine was dissolved in toluene (20 mL g⁻¹+volume of the Dean–Stark trap), CSA (1.0 equiv) was added, and the mixture was heated at reflux for 20 min. Afterwards, the required phenylacetaldehyde (1.2 equiv per reactive functional group) was added, and heating at reflux was continued in apparatus fitted with a Dean–Stark trap. After termination of the reaction, the mixture was extracted with toluene. The organic layer was dried over anhydrous MgSO₄, filtered, the solvent was removed, and the residue purified by column chromatography.

Compound 1b: TPA (0.5 g, 2.04 mmol), CSA (0.47 g, 2.04 mmol), and bis(4-methoxyphenyl)acetaldehyde (1.88 g, 7.34 mmol) were used (reaction time = 10 h). After extraction (toluene), the crude product was purified by column chromatography (2:23 acetone/*n*-hexane) to give **1b** (1.5 g, 77 %) as a bright-yellow powder. ¹H NMR (300 MHz, CDCl₃, 25 °C, TMS): $\delta=7.34\text{--}6.73$ (m, 35H), 6.67 (d, $J=7.2$ Hz, 4H), 3.87–3.68 ppm (m, 18H); ¹³C NMR (75 MHz, CDCl₃, 25 °C, TMS): $\delta=145.7$, 140.4, 136.7, 133.2, 132.5, 131.8, 131.6, 130.9, 130.4, 128.8, 128.3, 126.4, 125.9, 124.5, 124.0, 123.6, 114.3, 113.7, 113.6, 55.4 ppm; elemental analysis calcd (%) for C₆₆H₅₇NO₆: C 82.56, H 5.98, N 1.46; found: C 82.43, H 5.85, N 1.59.

Compound 2b: 4-Methyltriphenylamine (0.5 g, 1.93 mmol), CSA (0.45 g, 1.93 mmol), and bis(4-methoxyphenyl)acetaldehyde (1.19 g, 4.63 mmol) were used (reaction time = 6 h). After extraction (toluene), the crude product was purified by column chromatography (3:22 acetone/*n*-hexane) to give **2b** (0.99 g, 70 %) as a bright-yellow powder. ¹H NMR (300 MHz, CDCl₃, 25 °C, TMS): $\delta=7.29\text{--}6.94$ (m, 16H), 6.92–6.84 (m, 4H), 6.82 (s, 2H), 6.80–6.74 (m, 8H), 3.81–3.72 (m, 12H), 2.31–2.27 ppm (m, 3H); ¹³C NMR (75 MHz, CDCl₃, 25 °C, TMS): $\delta=159.2$, 158.3, 146.1, 144.8, 140.1, 137.9, 136.8, 133.2, 131.6, 130.8, 130.2, 128.7, 128.2, 125.9, 125.6, 123.2, 122.7, 114.3, 113.8, 113.6, 55.4, 21.1 ppm; elemental analysis calcd (%) for C₅₁H₄₅NO₄: C 83.24, H 6.16, N 1.90; found: C 83.39, H 6.07, N 1.72.

Compound 3b: 4,4'-Dimethyltriphenylamine (0.5 g, 1.83 mmol), CSA (0.42 g, 1.83 mmol), and bis(4-methoxyphenyl)acetaldehyde (0.56 g, 2.2 mmol) were used (reaction time = 6 h). After extraction (toluene), the crude product was purified by column chromatography (3:22 acetone/*n*-hexane) to give **3b** (0.7 g, 75 %) as a bright-yellow powder. M.p. 167–169 °C; ¹H NMR (300 MHz, CDCl₃, 25 °C, TMS): $\delta=7.23$ (d, $J=8.9$ Hz, 2H), 7.13 (d, $J=8.7$ Hz, 2H), 6.99 (dd, $J=22.7$, 8.4 Hz, 8H), 6.91–6.71 (m, 9H), 3.80 (d, $J=6.5$ Hz, 6H), 2.28 ppm (s, 6H); ¹³C NMR (75 MHz, CDCl₃, 25 °C, TMS): $\delta=159.1$, 159.0, 146.7, 145.2, 139.7, 136.8, 133.3, 132.8, 131.6, 131.0, 130.2, 130.0, 128.7, 126.1, 125.0, 121.5, 114.3, 113.7, 55.4, 21.0 ppm; elemental analysis calcd (%) for C₃₆H₃₃NO₂: C 84.51, H 6.50, N 2.74; found: C 84.34, H 6.63, N 2.89.

Compound 1c: TPA (0.5 g, 2.04 mmol), CSA (0.47 g, 2.04 mmol), and 2-phenylpropionaldehyde (0.98 g, 7.34 mmol) were used (reaction time = 5 h). After extraction (toluene), the crude product was purified by

column chromatography (1:49 THF/*n*-hexane) to give **1c** (0.86 g, 71%) as a yellow powder. ¹H NMR (300 MHz, CDCl₃, 25 °C, TMS): δ = 7.59–7.43 (m, 5H), 7.41–7.19 (m, 15H), 7.16 (d, *J* = 8.6 Hz, 3H), 7.06 (d, *J* = 8.5 Hz, 2H), 6.91–6.69 (m, 5H), 2.38–2.13 ppm (m, 9H); ¹³C NMR (75 MHz, CDCl₃, 25 °C, TMS): δ = 146.0, 144.5, 137.9, 136.7, 133.1, 130.3, 129.9, 128.8, 128.5, 127.5, 126.2, 123.9, 123.6, 17.9 ppm; elemental analysis calcd (%) for C₄₅H₃₉N: C 91.02, H 6.62, N 2.36; found: C 91.27, H 6.51, N 2.22.

Compound 2c: 4-Methyltriphenylamine (0.5 g, 1.93 mmol), CSA (0.45 g, 1.93 mmol), and 2-phenylpropionaldehyde (0.62 g, 4.63 mmol) were used (reaction time = 5 h). After extraction (toluene), the crude product was purified by column chromatography (1:249 acetone/*n*-hexane) to give **2b** (0.54 g, 57%) as yellow oil. ¹H NMR (300 MHz, CDCl₃, 25 °C, TMS): δ = 7.55–7.45 (m, 3H), 7.35 (t, *J* = 7.4 Hz, 3H), 7.30–7.16 (m, 7H), 7.14–6.94 (m, 8H), 6.82–6.69 (m, 3H), 2.38–2.12 ppm (m, 9H); ¹³C NMR (75 MHz, CDCl₃, 25 °C, TMS): δ = 146.4, 145.1, 144.5, 136.4, 133.4, 132.5, 130.2, 130.1, 129.8, 128.8, 128.5, 128.3, 127.6, 127.2, 126.2, 125.5, 123.2, 122.8, 21.1, 17.9 ppm; elemental analysis calcd (%) for C₃₇H₃₃N: C 90.39, H 6.77, N 2.85; found: C 90.53, H 6.49, N 2.98.

Compound 3c: 4,4'-Dimethyltriphenylamine (0.5 g, 1.83 mmol), CSA (0.42 g, 1.83 mmol), and 2-phenylpropionaldehyde (0.29 g, 2.2 mmol) were used (reaction time = 3 h). After extraction (toluene), the crude product was purified by column chromatography (1:249 acetone/*n*-hexane) to give **3c** (0.52 g, 73%) as yellow oil. ¹H NMR (300 MHz, CDCl₃, 25 °C, TMS): δ = 7.53–7.46 (m, 2H), 7.35 (t, *J* = 7.4 Hz, 2H), 7.29–7.18 (m, 3H), 7.09–6.98 (m, 8H), 6.95–6.90 (m, 1H), 6.76–6.71 (m, 2H), 2.33–2.14 ppm (m, 9H); ¹³C NMR (75 MHz, CDCl₃, 25 °C, TMS): δ = 146.8, 145.4, 144.6, 136.1, 132.7, 131.8, 130.1, 130.0, 128.5, 127.7, 127.1, 126.1, 124.9, 122.3, 21.0, 17.9 ppm; elemental analysis calcd (%) for C₂₉H₂₇N: C 89.42, H 6.99, N 3.60; found: C 89.50, H 7.10, N 3.40.

Acknowledgements

This research was supported by the European Social Fund under the Global Grant measure (VP1–3.1-ŠMM-07K 01–078). G.B. acknowledges EU Structural Funds project “Postdoctoral Fellowship Implementation in Lithuania” for funding her postdoctoral fellowship.

- [1] a) S. R. Forrest, *Nature* **2004**, *428*, 911; b) U. Mitschke, P. Bäuerle, *J. Mater. Chem.* **2000**, *10*, 1471; c) H. Spanggaard, F. C. Krebs, *Solar Energy Mater. Solar Cells* **2004**, *83*, 125; d) C. D. Dimitrakopoulos, P. R. L. Malenfant, *Adv. Mater.* **2002**, *14*, 99; e) D. S. Weiss, M. Abkowitz, *Chem. Rev.* **2010**, *110*, 479.
- [2] S. Allard, M. Forster, B. Souharce, H. Thiem, U. Scherf, *Angew. Chem.* **2008**, *120*, 4138; *Angew. Chem. Int. Ed.* **2008**, *47*, 4070.
- [3] E. Menard, V. Podzorov, S.-H. Hur, A. Gaur, M. E. Gershenson, J. A. Rogers, *Adv. Mater.* **2004**, *16*, 2097.
- [4] a) M. Halik, H. Klauk, U. Zschieschang, G. Schmid, W. Radlik, S. Ponomarenko, S. Kirchmeyer, W. Weber, *J. Appl. Phys.* **2003**, *93*, 2977; b) M. Halik, H. Klauk, U. Zschieschang, G. Schmid, W. Radlik, S. Ponomarenko, S. Kirchmeyer, W. Weber, *Adv. Mater.* **2003**, *15*, 917.
- [5] Y. Shirota, H. Kageyama, *Chem. Rev.* **2007**, *107*, 953.
- [6] P. Stroehriegel, J. V. Grazulevicius, *Adv. Mater.* **2002**, *14*, 1439.
- [7] P. M. Borsenberger, L. Pautmeier, R. Richert, H. Bässler, *J. Chem. Phys.* **1991**, *94*, 8276.
- [8] J. Veres, S. D. Ogier, S. W. Leeming, D. C. Cupertino, S. M. Khaffaf, *Adv. Funct. Mater.* **2003**, *13*, 199.
- [9] M. Sonntag, K. Kreger, D. Hanft, P. Stroehriegel, S. Setayesh, D. de Leeuw, *Chem. Mater.* **2005**, *17*, 3031.
- [10] T. Malinauskas, D. Tomkute-Luksiene, M. Daskeviciene, V. Jankauskas, G. Juska, V. Gaidelis, K. Arlauskas, V. Getautis, *Chem. Commun.* **2011**, *47*, 7770.
- [11] a) M. Sasaki (Ricoh Company Ltd.), US Patent US 4859556, **1989**; b) K. Nagai, M. Sasaki, H. Tamura, T. Suzuki, T. Shimada, C. Adachi, C. Tanaka, A. Katayama, N. Tamoto, K. Kishida, M. Anzai, A. Imai (Ricoh Company Ltd., Hodogaya Chemical Co., Ltd.), Jpn. Kokai Tokkyo Koho JP 09278723, **1997**; c) M. Sasaki (Ricoh Company Ltd.), Ger. Offen. DE 3414141, **1984**.
- [12] a) J. M. Plater, T. Jackson, *Tetrahedron* **2003**, *59*, 4673; b) M. V. Nandakumar, J. G. Verkade, *Angew. Chem.* **2005**, *117*, 3175; *Angew. Chem. Int. Ed.* **2005**, *44*, 3115.
- [13] a) H. J. Snaith, L. Schmidt-Mende, *Adv. Mater.* **2007**, *19*, 3187; b) J.-H. Yum, P. Chen, M. Grätzel, M. K. Nazeeruddin, *ChemSusChem* **2008**, *1*, 699; c) G. K. Mor, S. Kim, M. Paulose, O. K. Varghese, K. Shankar, J. Basham, C. A. Grimes, *Nano Lett.* **2009**, *9*, 4250; d) H. J. Snaith, A. J. Moule, C. Klein, K. Meerholz, R. H. Friend, M. Grätzel, *Nano Lett.* **2007**, *7*, 3372.
- [14] a) G. Meijer, G. Berden, W. L. Meerts, H. E. Hunziker, M. S. de Vries, H. R. Wendt, *Chem. Phys.* **1992**, *163*, 209; b) A. K. Bansal, A. Penzkofer, *Chem. Phys.* **2008**, *352*, 48.
- [15] R. Karpicz, S. Puzinas, S. Krotkus, K. Kazlauskas, S. Jursenas, J. V. Grazulevicius, S. Grigalevicius, V. Gulbinas, *J. Chem. Phys.* **2011**, *134*, 204508.
- [16] a) K. Itami, Y. Ohashi, J. Yoshida, *J. Org. Chem.* **2005**, *70*, 2778; b) H. Tong, Y. Dong, Y. Hong, M. Haussler, J. W. Y. Lam, H. H.-Y. Sung, X. Yu, J. Sun, I. D. Williams, H. S. Kwok, B. Z. Tang, *J. Phys. Chem. C* **2007**, *111*, 2287.
- [17] a) E. Montrimas, V. Gaidelis, A. Pazera, *Lith. J. Phys.* **1966**, *6*, 569; b) S. M. Vaezi-Nejad, *Int. J. Electron.* **1987**, *62*, 361; c) Y. Archie, C. Chan, C. Juhasz, *Int. J. Electron.* **1987**, *62*, 625.
- [18] a) Y. Shirota, K. Okumoto, H. Inada, *Synth. Met.* **2000**, *111–112*, 387; b) K. Okumoto, K. Wayaku, T. Noda, H. Kageyama, Y. Shirota, *Synth. Met.* **2000**, *111–112*, 473; c) A. Higuchi, K. Ohnishi, S. Nomura, H. Inada, Y. Shirota, *J. Mater. Chem.* **1992**, *2*, 1109; d) Y. Shirota, Y. Kuwabara, H. Inada, T. Wakimoto, H. Nakada, Y. Yonemoto, S. Kawami, K. Imai, *Appl. Phys. Lett.* **1994**, *65*, 807; e) Q.-X. Tong, S.-L. Lai, M.-Y. Chan, K.-H. Lai, J.-X. Tang, H.-L. Kwong, C.-S. Lee, S.-T. Lee, *Chem. Mater.* **2007**, *19*, 5851.
- [19] a) H. E. Katz, Z. Bao, *J. Phys. Chem. B* **2000**, *104*, 671; b) R. C. Haddon, X. Chi, M. E. Itkis, J. E. Anthony, D. L. Eaton, T. Siegrist, C. C. Mattheus, T. T. M. Palstra, *J. Phys. Chem. B* **2002**, *106*, 8288.
- [20] Y. Olivier, V. Lemaire, J. L. Bredas, J. Cornil, *J. Phys. Chem. A* **2006**, *110*, 6356.
- [21] a) A. M. van de Craats, N. Stutzmann, O. Bunk, M. M. Nielsen, M. Watson, K. Müllen, H. D. Chanzy, H. Sirringhaus, R. H. Friend, *Adv. Mater.* **2003**, *15*, 495; b) Z. An, J. Yu, S. C. Jones, S. Barlow, S. Yoo, B. Domercq, P. Prins, L. D. A. Siebbeles, B. Kippelen, S. R. Marder, *Adv. Mater.* **2005**, *17*, 2580; c) K. O. Sylvester-Hvid, *J. Phys. Chem. B* **2006**, *110*, 2618; d) A. R. Murphy, J. S. Liu, C. Luscombe, D. Kavulak, J. M. J. Fréchet, R. J. Kline, M. D. McGehee, *Chem. Mater.* **2005**, *17*, 4892.
- [22] a) M. Kirkus, M. H. Tsai, J. V. Grazulevicius, C. C. Wu, L. C. Chi, K. T. Wong, *Synth. Met.* **2009**, *159*, 729; b) E. Miyamoto, Y. Yamaguchi, M. Yokoyama, *Electrophotography* **1989**, *28*, 364; c) M. Cardona, L. Ley, *Top. Appl. Phys.* **1978**, *26*, 1.
- [23] T. Kodera, K. Torizuka (Mitsubishi Paper Mills, Ltd.), Jpn. Kokai Tokkyo Koho JP 11043458, **1999**.
- [24] M. J. Adams, J. G. Highfield, G. F. Kirkbright, *Anal. Chem.* **1977**, *49*, 1850.
- [25] J. C. de Mello, H. F. Wittmann, R. H. Friend, *Adv. Mater.* **1997**, *9*, 230.
- [26] a) S. Urnikaitė, T. Malinauskas, V. Gaidelis, R. Maldzius, V. Jankauskas, V. Getautis, *Carbon* **2011**, *49*, 320; b) D. Tomkute-Luksiene, T. Malinauskas, M. Daskeviciene, V. Gaidelis, R. Maldzius, J. Sidaravičius, V. Getautis, *Synth. Met.* **2011**, *161*, 1177; c) J. Kalade, E. Montrimas, R. Maldzius, Z. Tokarski, *J. Imaging Sci. Technol.* **2005**, *49*, 28.

Received: November 13, 2012

Revised: July 29, 2012

Published online: September 17, 2013